

Article

# A Simulation-Based Framework to Determine the Kinematic Compatibility of an Augmentative Exoskeleton during Walking

S. Nagarajan <sup>1,\*</sup>, K. Mohanavelu <sup>1</sup> and S. Sujatha <sup>2</sup> 

<sup>1</sup> Defence Bioengineering and Electromedical Laboratory (DEBEL), DRDO, MoD, Bengaluru 560093, Karnataka, India; mohanvelk.debel@gov.in

<sup>2</sup> Department of Mechanical Engineering, Indian Institute of Technology Madras, Chennai 600036, Tamil Nadu, India; sujsree@iitm.ac.in

\* Correspondence: nagarajans.debel@gov.in

**Abstract:** Augmentative exoskeletons (AEs) are wearable orthotic devices that, when coupled with a healthy individual, can significantly enhance endurance, speed, and strength. Exoskeletons are function-specific and individual-specific, with a multitude of possible configurations and joint mechanisms. This complexity presents a challenging scenario to quantitatively determine the optimal choice of the kinematic configuration of the exoskeleton for the intended activity. A comprehensive simulation-based framework for obtaining an optimal configuration of a passive augmentative exoskeleton for backpack load carriage during walking is the theme of this research paper. A musculoskeletal-based simulation approach on 16 possible kinematic configurations with different Degrees of Freedom (DoF) at the exoskeleton structure's hip, knee, and ankle joints was performed, and a configuration with three DoF at the hip, one DoF at the knee, three DoF at the ankle was quantitatively chosen. The Root Mean Square of Deviations (RMSD) and Maximum Deviations (MaxDev) between the kinematically coupled human–exoskeleton system were used as criteria along with the Cumulative Weight Score (CWS). The chosen configuration from the simulation was designed, realised, and experimentally validated. The error of the joint angles between the simulation and experiments with the chosen configuration was less than 3° at the hip and ankle joints and less than 6° at the knee joints.

**Keywords:** exoskeletons; kinematic compatibility; biomechanical simulation; musculoskeletal modelling; passive exoskeleton



**Citation:** Nagarajan, S.; Mohanavelu, K.; Sujatha, S. A Simulation-Based Framework to Determine the Kinematic Compatibility of an Augmentative Exoskeleton during Walking. *Robotics* **2024**, *13*, 79. <https://doi.org/10.3390/robotics13050079>

Academic Editors: Kean Aw and Dan Zhang

Received: 4 March 2024

Revised: 26 April 2024

Accepted: 9 May 2024

Published: 17 May 2024



**Copyright:** © 2024 by the authors. Licensee MDPI, Basel, Switzerland. This article is an open access article distributed under the terms and conditions of the Creative Commons Attribution (CC BY) license (<https://creativecommons.org/licenses/by/4.0/>).

## 1. Introduction

Exoskeletons find tremendous applications in strength augmentation, primarily in military scenarios [1], mobilisation of Spinal Cord Injury (SCI) patients in rehabilitation [2], and industrial applications for injury prevention while enhancing endurance [3]. Exoskeletons are external structural devices connected to the human through interfaces that can provide homogenous movements coupled with the wearer.

Human movement, which has evolved over millions of years [4], is highly adaptable to perform a broad spectrum of biomechanical activities and can efficiently engage with the external environment. A complex combination of different muscles is triggered to minimise time, effort, and energy or maximise power to achieve the intended movement. Therefore, one exoskeleton configuration may not suffice for all biomechanical activities.

Exoskeletons' system architecture is always function-specific and individual-specific. They are classified as upper-extremity exoskeletons [5], lower-extremity exoskeletons [2,6,7], or full-body exoskeletons. Under each category, there are powered exoskeletons and unpowered/passive exoskeletons. Passive exoskeleton systems perform the intended function using mechanical and compliant elements [8].

Augmentative exoskeletons (AEs) coupled with healthy individuals augment their capability by enhancing endurance and increasing strength without compromising mobility [9]. Unlike a rehabilitative exoskeleton, an AE requires the system to move synchronously with the wearer to provide significant augmentation. Several challenges must be overcome in developing an AE system [10,11]. Most of these challenges fundamentally arise from the wearer's perceived comfort of the Human–Machine Interface (HMI). Kinematic incompatibility is an important limiting factor inhibiting research prototypes from transforming into large-scale deployable functional exoskeletons. The rigidity and stiffness of the structural elements of the exoskeleton, coupled with a complaint of the human body, lead to a mismatch between the motions of the human and the exoskeleton. This drastically reduces the augmentative capability of the system. Hence, human–exoskeleton synchronisation is the key to enhancing augmentation. Minimisation of the human–exoskeleton misalignment has rarely been explored in a quantifiable manner in the literature [12]. However, subject-specific kinematic modelling has been performed to predict human motion in rehabilitative-powered exoskeleton systems [13].

The exoskeleton systems are connected in parallel or series with the human structure to achieve the intended function [14,15]. When the systems are connected in parallel to the human limbs and torso, the exoskeleton joints should provide the same Range of Motion (RoM) and align with the human joints continuously during the complete biomechanical activity. Misalignment of human and exoskeleton joints leads to increased interaction forces at the HMI, resulting in decreased comfort, increased effort, and metabolic cost, significantly reducing the system's efficacy. An exoskeleton asynchronous with the wearer's movement will impede the motion and adversely hamper the primary objective of augmentation. Yandell et al. [16] reported a decrease of 50% in useful assistive torque and an increase in forces at the HMI in unintentional directions due to kinematic misalignment.

At the same time, it is nearly impossible to accurately replicate the human system with joints having moving axes of rotation and the range of motion for all the activities. Human joints are covered with soft tissues, and hence, the exact location of the joint centres is difficult to estimate. The mechanical joints of the exoskeletons are designed to provide adequate RoM and maintain the axis' alignment in the best possible manner. There are primarily three strategies concerning misalignment compensation, as suggested by Naf et al. [17], to minimise the kinematic incompatibility, with each strategy having its advantages and limitations.

The first common approach has been to reduce misalignment by introducing compliant elements at the various joints of the exoskeleton [18]. The strategy provides kinematic redundancy but increases the design complexity of the exoskeleton. Another novel approach is the introduction of Self-Aligning Mechanism (SAM) joints as proposed by Stienen et al. and Cempini M et al. [19,20]. Accurate initial adjustment of the exoskeleton is not necessary while using SAM. Still, suppose the mechanism is displaced beyond its workspace (due to slippage or the cumulative effect of misalignments of other joints) in the serial kinematic chain. In that case, it may become ineffective in preventing misalignment. Other studies have introduced extra Degrees of Freedom (DoF) to the exoskeleton joints [21,22] at the interface or joint levels to reduce misalignments. However, this increases the overall complexity and weight of the exoskeleton when it encompasses many of the wearer's joints. As Zanotto et al. [23] reported, it is essential to find the best trade-off between a complex architecture, which may be misalignment-free theoretically but bulky and cumbersome for customisation to the wearer, and a more straightforward, traditional design with limited complexity, friction, and inertia.

Even after adopting these strategies, the fitment of the exoskeleton and its alignment to the human joints dramatically depend on the individual's skill, which further leads to intra/inter-subject variability of the individual trained for fitment. The exoskeletons are manually aligned to the human subject during a static posture like standing, whereas the functional requirement may be completely different. During dynamic movements, there is

a continuous change in the human joint axis position and orientation, leading to increased misalignment between the human–exoskeleton coupled system.

This research envisages a novel subject-specific musculoskeletal-based simulation framework to realise the best kinematically compatible solution (among the options considered with simple joints) of a passive augmentative exoskeleton during walking. This approach uses subject-specific experimental reference data, such as positions of anatomical joint centres and orientations of the human segment, to scale an anthropomorphic skeletal model and align the human–exoskeleton system. The intended outcome aims to answer the following two research questions. (a) What should be the best kinematic configuration of a passive augmentative exoskeleton intended for backpack load carriage during walking? (b) Is it possible to have a generic simulation-based approach to identify the ideal kinematic configuration for such systems?

This paper attempts to fill the research gap using a musculoskeletal simulation-based framework. Musculoskeletal system modelling has evolved only during the last decade. All musculoskeletal modelling platforms require motion capture data as an input to drive the mathematical model of the human. Hence, the kinematics of human walking were captured using an Inertial Measurement Unit (IMU) system. The capability to integrate IMU-based kinematic measurements [24] was made available recently [25]. The kinematic measurement of the individual and a virtual model of the exoskeleton are exported into a musculoskeletal simulation environment. Human exoskeleton systems are kinematically coupled at the various interfaces of human segments and exoskeleton straps. The human–exoskeleton coupled inverse kinematics are simulated for various configurations using subject-specific reference data, and the best configuration was chosen. Joint misalignments have been used as a metric to obtain the best configuration without estimating the interaction forces. A prototype was physically realised based on the simulations.

Further, experimental validation of kinematic compatibility was performed by simultaneously measuring the kinematics of the wearer and exoskeleton during walking and comparing these with simulation results. This methodology would reduce the iterations in the product development lifecycle to obtain the best kinematic configuration. The literature does not explicitly use simulations to assess kinematic incompatibility utilising the combination of IMU-based measurements and musculoskeletal modelling.

Hence, this simulation-based framework is generic and suitable for any type of augmentative exoskeleton (powered/passive) and any biomechanical activity. External actuation (torque/force) can be provided to the joints of the human/exoskeleton in the musculoskeletal simulation platform to simulate a powered system. The human–exoskeleton coupled simulation-based approach could be extended to other compensation strategies to minimise misalignments, such as introducing redundant kinematic links and joints.

## 2. Materials and Methods

The aim is to develop a simulation-based framework to find the best kinematic configuration of a passive augmentative exoskeleton for the lower extremities coupled with a healthy subject during walking. The volunteer was recruited after an informed consent form was explained and signed. The criteria for recruitment were that the volunteer should be physically fit with good exercise tolerance, between 150 and 190 cm of height, with no history of cardiovascular issues, respiratory issues, back pain, or surgery. The subject recruited for the study was 36 years old (height 184 cm) with no record of lower extremity injuries. The joint kinematics data used for simulation and experimental validation was performed on the same subject. Virtual 3D modelling of the different configurations of exoskeletons, as detailed in Table 1, was realised in SolidWorks® 2018. This was coupled with the TLEM 2.0 human model [26] in the AnyBody Modelling System v.7.3.2 (AMS) (AnyBody Modelling System A/S, Aalborg, Denmark) [27]. Walking of a human model in AMS was simulated using kinematic data obtained from Xsens MVN Awinda (2020) (XSens Technologies, Enschede, The Netherlands) [28] at a sampling rate of 60 Hz. The exoskeleton was coupled with the human model in AMS and initially matched with the

standing data in the sagittal plane with the human anatomical joint centres. Subsequently, the joint kinematics during walking drives the human model coupled with the exoskeleton. The kinematic error between the exoskeleton and human joint angles was analysed for different configurations to obtain the best kinematic configuration during walking.

**Table 1.** Different kinematic configurations of the lower extremity exoskeleton studied here.

| No        | Total DoF | Added DoFs to Flexion/Extension at the Hip, Knee, and Ankle Joints.  |
|-----------|-----------|--|
| Config 1  | 6         | -  |
| Config 2  | 8         | Ankle Inversion/Eversion   |
| Config 3  | 8         | Ankle Internal/External Rotation   |
| Config 4  | 10        | Ankle Inversion/Eversion; Ankle Internal/External Rotation   |
| Config 5  | 8         | Hip Abduction/Adduction  |
| Config 6  | 8         | Hip Internal/External Rotation   |
| Config 7  | 10        | Hip Abduction/Adduction; Ankle Inversion/Eversion  |
| Config 8  | 10        | Hip Abduction/Adduction; Ankle Internal/External Rotation  |
| Config 9  | 10        | Hip Internal/External Rotation; Ankle Inversion/Eversion   |
| Config 10 | 10        | Hip Internal/External Rotation; Ankle Internal/External Rotation   |
| Config 11 | 12        | Hip Abduction /Adduction; Ankle Inversion/Eversion; Ankle Internal/External Rotation                                 |
| Config 12 | 12        | Hip Internal/External Rotation; Ankle Inversion/Eversion; Ankle Internal/External Rotation                           |
| Config 13 | 10        | Hip Abduction/Adduction; Hip Internal/External Rotation  |
| Config 14 | 12        | Hip Abduction /Adduction; Hip Internal/External Rotation; Ankle Internal/External Rotation                           |
| Config 15 | 12        | Hip Abduction /Adduction; Hip Internal/External Rotation; Ankle Inversion/Eversion                                   |
| Config 16 | 14        | Hip Abduction /Adduction; Hip Internal/External Rotation; Ankle Inversion/Eversion; Ankle Internal/External Rotation |

The human model in AMS has three DoFs at the hip joint, one at the knee joint, and two at the ankle joint. The RoM of the knee joint, flexion/extension (F/E), is predominant during walking, and hence, the exoskeleton knee joint is approximated to a one-DoF hinge joint in the sagittal plane. The human ankle joint has two DoF: dorsi-flexion and plantar-flexion (DF/PF) and inversion/eversion (In/Ev).

As the intended biomechanical activity is walking, which mainly occurs in the sagittal plane, it is mandatory to have F/E at the hip, knee, and ankle joints of the exoskeleton combined with other DoF in the frontal and transverse planes at various joints. The hip joint F/E could be combined with abduction/adduction (Ab/Ad), internal rotation/external rotation (I/E), or all three DoFs could be used. Hence, the possible combinations of the hip joint at the hip are (i) hip (F/E), (ii) hip (F/E) (Ab/Ad), (iii) hip (F/E) (I/E), (iv) hip (F/E) (Ab/Ad) (I/E). While the knee joint of the exoskeleton offers only (F/E), the ankle joint with (DF/PF) could be combined with In/Ev, I/E, or both. Hence, the possible combinations of the ankle joint are (i) ankle (DF/PF), (ii) ankle (DF/PF) (In/Ev), (iii) ankle (DF/PF) (I/E), (iv) ankle (DF/PF) (In/Ev) (I/E).

As described in Table 1, there are sixteen plausible combinations of the hip, knee, and ankle joints for an exoskeleton. Flexion/extension of each hip, knee, and ankle joint is mandatory to achieve walking; hence, the combination is limited to 16. The joint DoFs of the exoskeleton configurations could vary from a minimum of 6 to a maximum of 14.

### 2.1. Kinematic Data Collection for Simulation and Analysis

The kinematic data were collected from Xsens Awinda during standing and walking when the subject walked on level ground for 10 m at an approximate speed of 2 kmph for nine gait cycles. One complete gait cycle from the heel strike of the left leg was chosen for simulation, and it occurred within 1.6 s in the musculoskeletal system AMS.

The Xsens system consists of a torso suit with adjustable straps encompassing 17 wireless IMU sensors fitted onto the body, as shown in Figure 1a. The joint kinematics of 23 segments and 22 joints are captured and analysed using MVN Analyze Pro software (2021.2.0). Figure 1b shows a flow chart from subject preparation to processing in AMS.

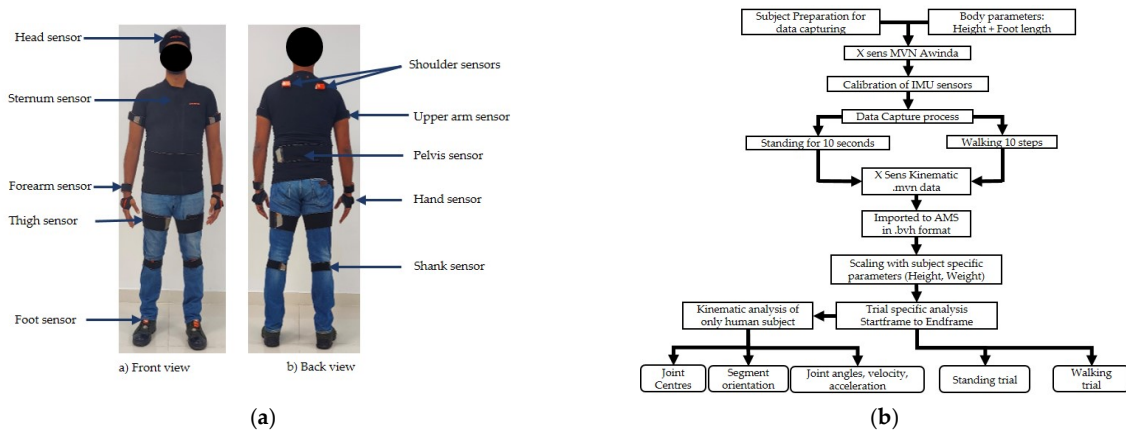


**Figure 1.** Functional representation of IMU sensor data collection and its analysis methodology. (a) IMU sensor configuration. (b) Flow chart: Data capture to simulation.

The output kinematic data, as shown in Figure 2, from Xsens during the complete gait cycle were obtained in .mvn format. They were further processed, exported in Bio Vision Hierarchy (.bvh) format, and scaled with AMS subject-specific parameters. The input reference trajectories drive the human model in AMS during walking. Subsequently, the virtual prototype of the exoskeleton is constrained and integrated with the AMS platform. The hip, knee, and ankle joint angles are simultaneously captured during walking and compared in the simulation environment.

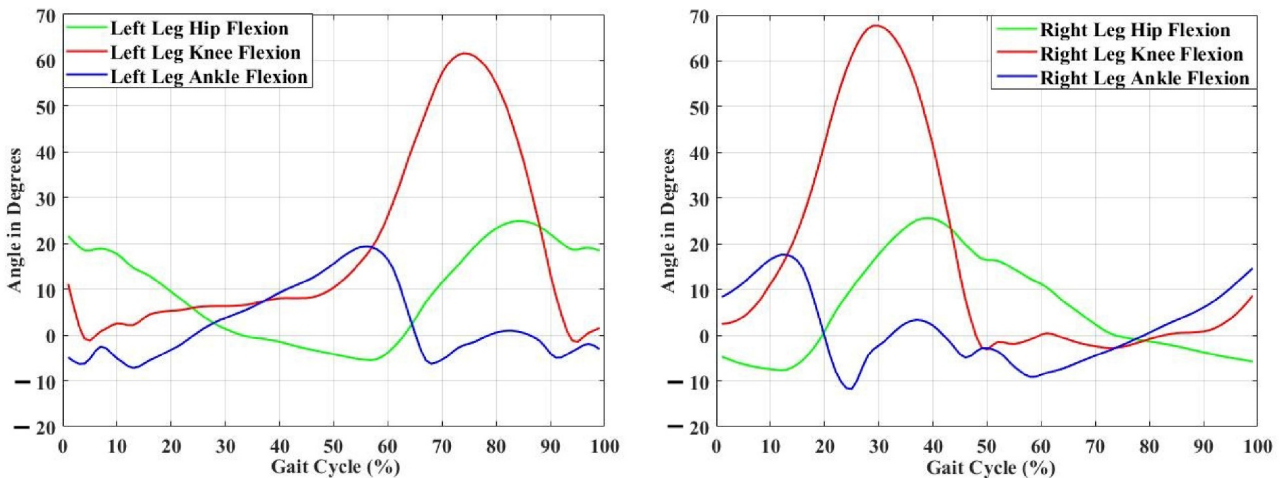


**Figure 2.** Joint angle kinematics (RoM) of hip, knee, and ankle of both legs for one gait cycle.

2.2. Constraining the Virtual Exoskeleton System with the Human Model in AMS

The captured kinematic data were processed in the musculoskeletal modelling platform AMS coupled with the exoskeleton environment model.

The human standing model considered for analysis has 72 segments and 122 joint DoF, as shown in Figure 3a. An individual-specific scaled skeletal model was obtained by importing the kinematic data from Xsens and initialising the scaling condition. The generic exoskeleton modelled in SolidWorks® 2018 was imported to AMS, as shown in Figure 3b. The inverse kinematics is obtained from the closed-loop kinematic solution of the solver after kinematically constraining the exoskeleton components with the AMS human body model, as shown in Figure 3c. A generic exoskeleton model consisting of seven components was modelled in SolidWorks® 2018 and then exported to AMS.

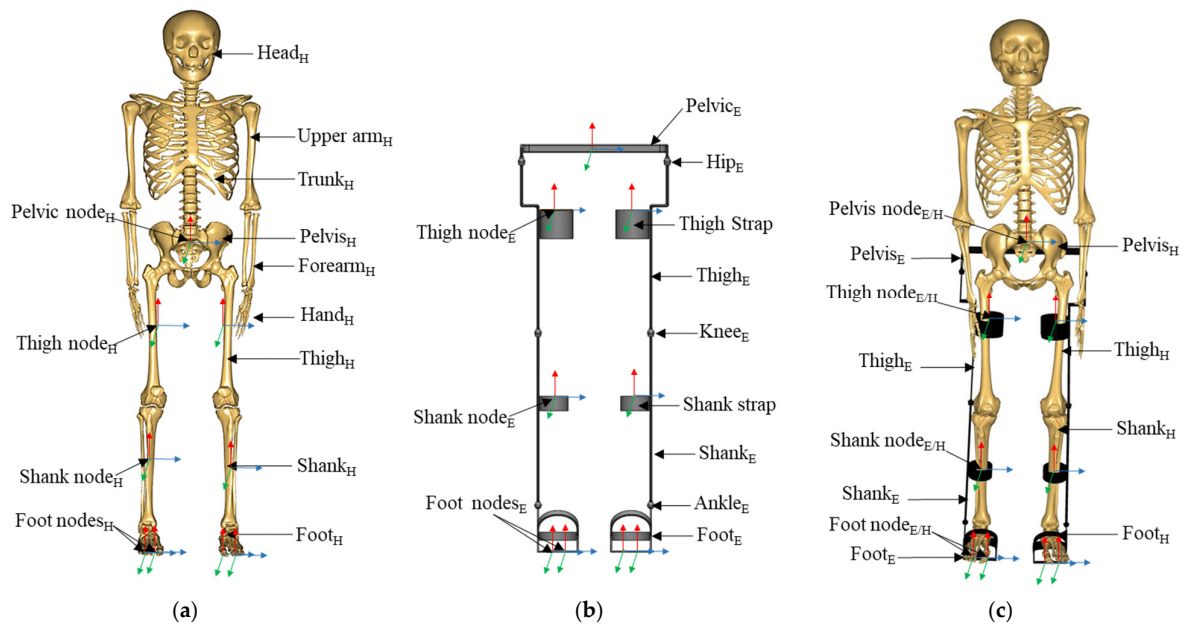


**Figure 3.** Human and exoskeleton models used in the simulations. (a) Standing human model. (b) Exoskeleton model (Config 16). (c) Exoskeleton integrated with human.

As shown in Figure 4, the exoskeleton is modelled as a set of seven components. Each component has a ball and socket on either extremity, with one node associated at each end. An extra node on each of the seven components constrains the associated human segment to simulate the straps. The seven components are appropriately constrained to obtain 16 different kinematic configurations of the exoskeleton structure, as described in Table 1.

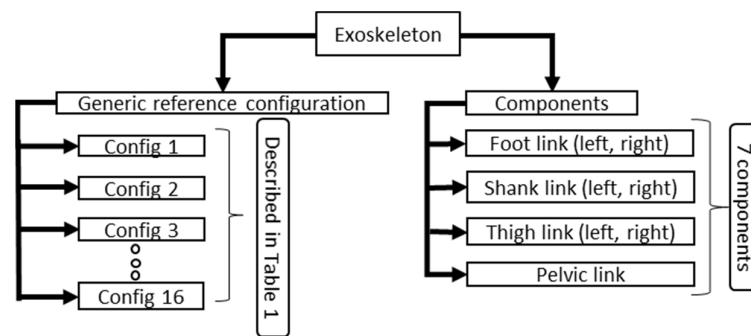


**Figure 4.** Generic model of exoskeleton with seven components for all configurations.

The orientations and the joint centres of the exoskeleton segments are matched to the orientations of the human segments during standing, and the same is verified in the sagittal plane. The constraints between the human and the exoskeleton are simulated according to the physical system being constrained with the straps at the human’s foot, shank, thighs, and waist. The human foot is wholly coupled with the exoskeleton foot link. Hence, all six DoF are arrested between the human and exoskeleton feet on the right and left. Subsequently, the shank links of the exoskeleton form the ankle joint with the foot link and the knee joint with the thigh link. Hence, the node representing the strap is soft-constrained for orientation with the human shank link. This allows for slight movement when the AMS algorithm attempts to solve the closed-loop kinematics of the human–exoskeleton coupled system. A similar strap constraint is given for the thigh strap and waist straps with the nodes on the thigh links and the waist link, respectively. After matching the exoskeleton with the standing model, walking simulations are performed.

### 2.3. Musculoskeletal Simulation Results

The coupled kinematics of the human exoskeleton system are solved in the musculoskeletal simulation platform for walking. The joint RoM for the human and exoskeleton models' hip, knee, and ankle are plotted for one gait cycle.

Figure 5 shows a typical output plot of the simulated RoM of the hip joint of the human and exoskeleton during the complete gait cycle.

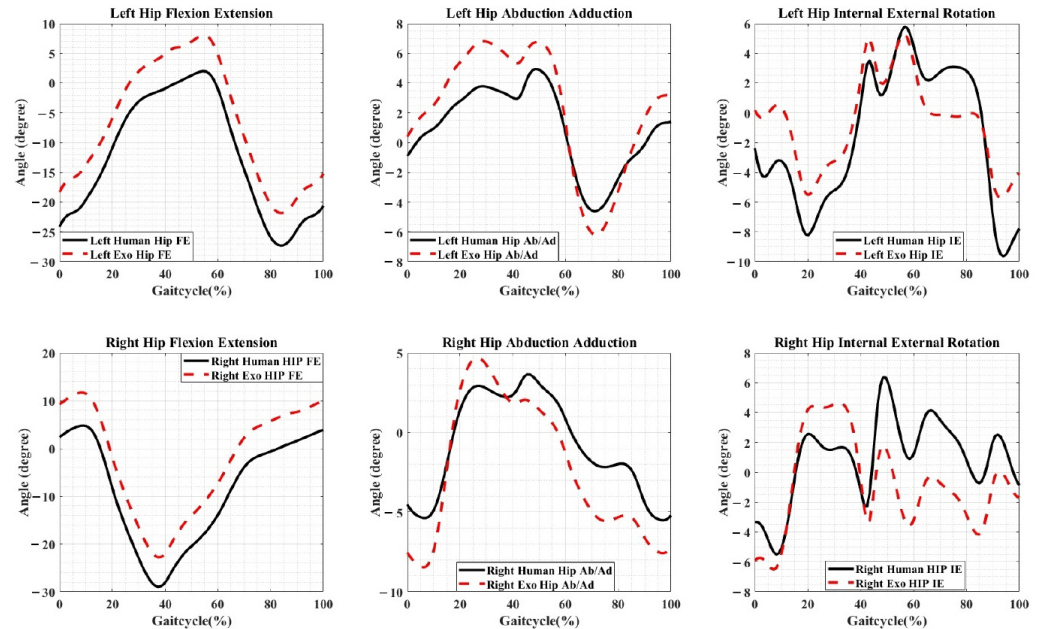


Figure 5. Typical simulation results of hip joint RoM of human and exoskeleton for configuration 16.

The Root Mean Square of Deviations (RMSD) and the Maximum Deviations (MaxDev) between human and exoskeleton joint kinematics are obtained for all joints (left and right legs) in all 16 configurations and tabulated in Table 2. The RoM of all joints (human and exoskeleton) for all 16 configurations are plotted in Figure S1 of the Supplementary Materials. The deviation profiles for all the configurations are plotted in Figure S2 of the Supplementary Materials.

Table 2. RMSD (MaxDev) between human and exoskeleton joint kinematics for all configurations. The numbers in green indicate the four lowest values in each column. The CWS is computed by adding the number of occurrences of values in green across a row. A higher CWS indicates a more suitable configuration.

| Configurations | Lhip Ab/Ad   | Lhip I/E     | Lhip F/E      | Rhip Ab/Ad   | Rhip I/E     | Rhip F/E      | Lknee F/E    | Rknee F/E    | Lankle F/E   | Lankle In/Ev  | Rankle F/E   | Rankle In/Ev  | CWS      |
|----------------|--------------|--------------|---------------|--------------|--------------|---------------|--------------|--------------|--------------|---------------|--------------|---------------|----------|
| Config1        | 1.5<br>(2.3) | 3.4<br>(4.6) | 5.5<br>(5.6)  | 1.7<br>(2.5) | 3.7<br>(4.7) | 6.3<br>(6.5)  | 0.6<br>(1)   | 0.7<br>(1)   | 0.5<br>(0.8) | 3.9<br>(5.9)  | 0.5<br>(1.6) | 3.9<br>(6.2)  | 6<br>(9) |
| Config2        | 2<br>(3.3)   | 3<br>(4.8)   | 5.4<br>(6.5)  | 1.9<br>(2.9) | 3.4<br>(4.8) | 6.3<br>(7.1)  | 2.2<br>(4.6) | 2.5<br>(4.7) | 1<br>(2.2)   | 1.8<br>(2.6)  | 1<br>(2.5)   | 1.8<br>(3.2)  | 3<br>(4) |
| Config3        | 1.9<br>(3.4) | 3.2<br>(5.4) | 5.6<br>(5.8)  | 1.9<br>(3.2) | 3.1<br>(5.2) | 6.4<br>(6.6)  | 0.8<br>(1.4) | 0.8<br>(1.4) | 0.6<br>(0.7) | 4.9<br>(10.4) | 0.6<br>(1.6) | 4.9<br>(10.5) | 3<br>(4) |
| Config4        | 2.1<br>(3.3) | 2.9<br>(5.1) | 1.2<br>(1.6)  | 1.7<br>(2.9) | 3.2<br>(5.3) | 0.6<br>(1.1)  | 1<br>(2.4)   | 1.8<br>(4)   | 0.8<br>(1.5) | 5.1<br>(11.2) | 0.8<br>(2.1) | 5.1<br>(12.1) | 4<br>(5) |
| Config5        | 2.1<br>(3.6) | 3.6<br>(6)   | 7.5<br>(10.8) | 2.6<br>(4.2) | 3.6<br>(6.4) | 7.2<br>(11.6) | 4.1<br>(6.4) | 3.6<br>(6.3) | 0.7<br>(1.5) | 4.2<br>(6.6)  | 0.7<br>(2.2) | 4.2<br>(6.5)  | 2<br>(1) |
| Config6        | 0.4<br>(1)   | 3.1<br>(4.7) | 5.2<br>(6.3)  | 1.5<br>(3.6) | 4.1<br>(5.9) | 6.1<br>(7.4)  | 1.1<br>(1.4) | 1.2<br>(2.1) | 1<br>(2.3)   | 4<br>(6.2)    | 1<br>(2.6)   | 4<br>(5.8)    | 4<br>(1) |

Table 2. Cont.

| Configurations | Lhip Ab/Ad   | Lhip I/E     | Lhip F/E      | Rhip Ab/Ad   | Rhip I/E      | Rhip F/E       | Lknee F/E    | Rknee F/E    | Lankle F/E    | Lankle In/Ev  | Rankle F/E    | Rankle In/Ev  | CWS      |
|----------------|--------------|--------------|---------------|--------------|---------------|----------------|--------------|--------------|---------------|---------------|---------------|---------------|----------|
| Config7        | 5.3<br>(9.9) | 4.5<br>(9)   | 12<br>(19.3)  | 4.9<br>(11)  | 6.8<br>(15.9) | 10.9<br>(18.7) | 3<br>(6.9)   | 3.1<br>(7.7) | 2.2<br>(6.6)  | 2.8<br>(4.7)  | 2.2<br>(4.4)  | 2.8<br>(4.1)  | 2<br>(2) |
| Config8        | 1.9<br>(3.4) | 3.6<br>(6.8) | 7.4<br>(10.7) | 2.5<br>(4.1) | 3.3<br>(6.7)  | 7.1<br>(11.6)  | 3.9<br>(6.1) | 3.6<br>(6.2) | 0.7<br>(1.6)  | 5.3<br>(10.2) | 0.7<br>(2.3)  | 5.3<br>(9.8)  | 2<br>(0) |
| Config9        | 1.5<br>(2.7) | 2.7<br>(5.2) | 5.6<br>(6.9)  | 2.7<br>(5.5) | 3.3<br>(4.9)  | 6.2<br>(8.4)   | 1.9<br>(3.8) | 1.8<br>(5.3) | 1.5<br>(3.4)  | 1.6<br>(3.8)  | 1.5<br>(11.2) | 1.6<br>(4.6)  | 5<br>(2) |
| Config10       | 1.6<br>(2.7) | 3.2<br>(5.9) | 5.8<br>(7.3)  | 2.2<br>(3.8) | 3.4<br>(5.3)  | 6.5<br>(7.8)   | 1.1<br>(2.3) | 1.4<br>(2.6) | 0.8<br>(2.2)  | 5<br>(10.3)   | 0.8<br>(1.8)  | 5<br>(10.2)   | 0<br>(1) |
| Config11       | 1.9<br>(3.2) | 3.4<br>(6.5) | 6.9<br>(10.6) | 2<br>(3.5)   | 3.3<br>(7.1)  | 7.1<br>(12)    | 3.5<br>(5.4) | 3.3<br>(5.7) | 0.8<br>(2.1)  | 5.9<br>(10.7) | 0.8<br>(2.8)  | 5.9<br>(13.9) | 0<br>(0) |
| Config12       | 1.5<br>(2.2) | 2.7<br>(5.1) | 5.4<br>(6.2)  | 1.7<br>(2.6) | 3<br>(4.9)    | 6.1<br>(6.9)   | 0.8<br>(1.9) | 1<br>(2.1)   | 1.3<br>(2)    | 5.4<br>(12.2) | 1.3<br>(2.2)  | 5.4<br>(12.5) | 6<br>(2) |
| Config13       | 1.6<br>(2.5) | 3.2<br>(4.5) | 5.5<br>(5.9)  | 2.1<br>(3)   | 3.7<br>(4.9)  | 6.3<br>(6.7)   | 0.7<br>(1.1) | 0.6<br>(1.2) | 0.8<br>(1.8)  | 3.4<br>(5.8)  | 0.8<br>(2.6)  | 3.4<br>(5.5)  | 2<br>(4) |
| Config14       | 1.6<br>(2.6) | 2.7<br>(4.4) | 5.4<br>(5.7)  | 2<br>(3.3)   | 3.2<br>(4.6)  | 6.2<br>(6.7)   | 0.6<br>(0.9) | 0.5<br>(0.9) | 0.9<br>(1.9)  | 4.3<br>(9.2)  | 0.9<br>(2.7)  | 4.3<br>(8.3)  | 6<br>(6) |
| Config15       | 3.3<br>(7.4) | 2.7<br>(4.5) | 6.6<br>(10)   | 4.3<br>(9.7) | 3.2<br>(5.1)  | 7.7<br>(11.9)  | 1.2<br>(2.7) | 1.2<br>(3.4) | 4.8<br>(12.6) | 3.1<br>(5.3)  | 4.8<br>(11.6) | 3.1<br>(5.3)  | 2<br>(2) |
| Config16       | 1.9<br>(3)   | 2.6<br>(4.1) | 5.5<br>(6)    | 2.2<br>(3.4) | 3.1<br>(4.8)  | 6.4<br>(7)     | 0.5<br>(0.7) | 0.6<br>(0.9) | 1.4<br>(2.2)  | 2.8<br>(5.2)  | 1.4<br>(3)    | 2.8<br>(7.5)  | 6<br>(5) |

#### 2.4. Determination of the Best Configuration of the Exoskeleton

The strategy used to determine the best configuration of the exoskeleton from Table 2 is as follows.

Step 1: For a given joint angle (each column of Table 2), the top 25 percentile of the configurations with minimum values of RMSD and MaxDev are identified, i.e., the least values are marked in green in each column until at least four configurations are determined.

Step 2: As identified from the first step, all the values of RMSD and MaxDev in the top 25 percentile of the configurations were assigned one weightage score (all values marked in green were assigned a weightage score of 1).

Step 3: Finally, the Cumulative Weight Score (CWS) was obtained by adding the number of instances of the entries in green (not the sum of absolute values for each configuration) and tabulated in the last column of Table 2.

Step 4: The top 25 percentile of the configurations with maximum CWS was considered, and the best configuration for the application, in this case, walking on uneven surfaces, was identified.

The higher CWS score results from higher occurrences of the least values of RMSD and MaxDev, demonstrating a better configuration. The higher the number of occurrences of a lower RMSD indicates a lower misalignment. Similarly, higher occurrences of a lower MaxDev value indicate a lesser deviation. Hence, the more instances where a particular configuration has the least RMSD and MaxDev values at various joints, the better the exoskeleton configuration.

From Table 2, based on the RMSD of the human–exoskeleton system, it is inferred that Config1, Config12, Config14, and Config16 are potential configurations with high CWS indices. On examining the MaxDev between the human and exoskeleton in Table 2, Config1, Config4, Config14, and Config16 are the potential configurations based on their high CWS indices.

As the exoskeleton is designed for walking on even and uneven surfaces, a suitable configuration mandates sufficient mobility at the hip and the ankle joint. Hence, Config 1 is eliminated as it has only F/E DoF at the hip, knee, and ankle joints. Considering the necessity of having Ab/Ad movement at the hip joint for mobility on uneven surfaces, Config 4 and Config 12 are eliminated. Further, considering the necessity of having Ab/Ad

movement at the ankle joint for mobility on uneven surfaces, Config 14 is eliminated. Hence, Config 16 is the most suitable candidate for high kinematic compatibility for walking on uneven surfaces and is selected as the most appropriate configuration for further realisation and experimentation.

Hence, out of the five optimal configuration options, the necessity of having the abduction/adduction motion at the hip and ankle joints was used as a criterion for elimination and obtaining the best configuration for walking on even and uneven surfaces [29,30]. The cumulative effects of having all possible combinations of DoFs in all three joints (hip, knee, ankle) can be quantitatively understood only from the complete simulation of all 16 configurations.

### 3. Development of Exoskeleton Prototype

The exoskeleton with the chosen configuration was designed, realised, and experimentally tested to validate the simulation-based framework. Experiments were performed on the same subject, wearing only the exoskeleton configuration obtained from the simulation. As the kinematic constraints between the human and exoskeleton systems remain the same for all configurations of the exoskeleton, the simulation provides an equally effective comparison of configurations. The kinematic diagram describing this configuration of the passive augmentative exoskeleton is shown in Figure 6a. The configuration with three DoF at the hip joint, one DoF at the knee joint, and three DoF at the ankle joint were designed and modelled, as shown in Figure 6b. The structure will have joints at the hip, knee, and ankle to mimic the motions of the anatomical joints during walking. Figure 6c shows that a spring–damper mechanism transfers the backpack load from the pelvic to the thigh link. However, as there is no load carriage in this analysis, the spring–damper system is in a transparent mode, equivalent to having no spring–damper at all, as it does not support any load or restrict any motion. The passive augmentative exoskeleton is attached to the human body at the foot, shank, thigh, and waist with their respective straps, as shown in Figure 6d.

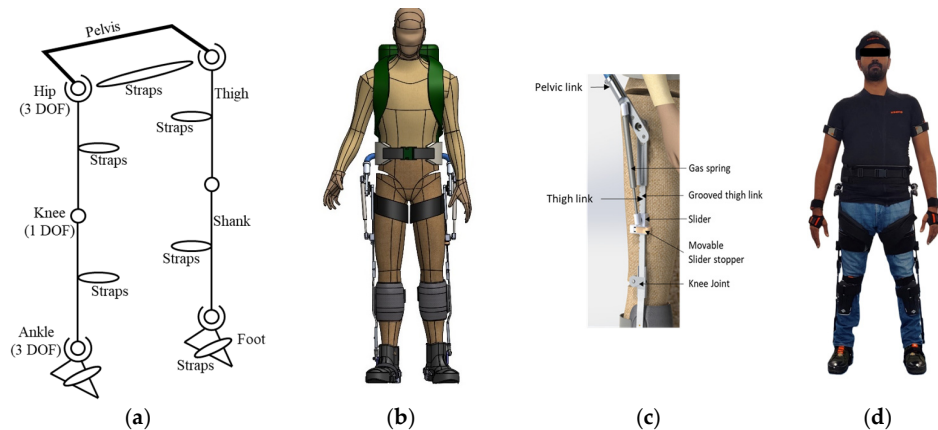


**Figure 6.** Development and realisation of exoskeleton prototype. (a) Kinematic configuration. (b) 3D model. (c) Spring damper system. (d) Prototype.

#### Experimental Setup for Validation

To evaluate and compare the kinematics of human walking with an exoskeleton, the kinematics of both the human and the exoskeleton must be captured separately but simultaneously using a trigger box. BTS trigger box time synchronises the motion data from the BTS motion capture system and the Xsens Awinda system. The trigger unit box sends an external start pulse to the BTS device and Xsens to start and stop the common data acquisition. The trigger unit box is used to manually generate the pulse. Initially, the trigger box is connected to the BTS mocap system. The output of the trigger box is connected to the sync-in port of the Xsens Awinda receiver system. When the trigger box start button is

pressed, Xsens and the BTS mocap system record the data simultaneously. When the stop button is pressed in the trigger box, the data recording in both systems stops.

Human kinematics is obtained by donning a full body protocol of sensors of the Xsens Awinda system, and exoskeleton kinematics is obtained by placing passive reflective markers and the motion captured by the infrared camera from the BTS system. The schematic of the experiment is shown in Figure 7.

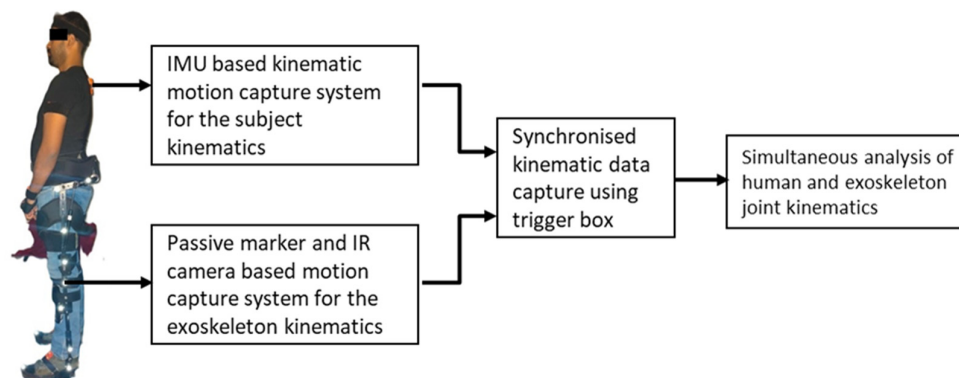


**Figure 7.** Schematic for human–exoskeleton simultaneous kinematic data collection.

Figure 8 shows the experimental setup for simultaneous kinematic data capture of the subject and exoskeleton. The subject is strapped with 17 IMU sensors from the Xsens Awinda system on the various body segments. The Xsens system is calibrated before data capture and measures the subject’s joint kinematics. Loosening of straps, slippage of sensors, and improper postponing of sensors on human segments lead to errors in kinematic data capture, data drifting, or unrealistic human movements. The system has to be recalibrated before data recording. Three non-collinear marker trajectories are captured using the BTS motion capture system on each exoskeleton component. The position and orientation of each exoskeleton segment are obtained, and the individual joint angles are calculated to show the difference between the segment orientations. The BTS wand calibration defines the system’s workspace. The challenges with a camera-based reflective marker system are marker occlusions, ghost markers, and limited capture volume. Hence, the exoskeleton is anodised black to prevent reflections and ghost markers. Good workspace calibration and marker placement at appropriate positions are ensured before data capture. Trajectories of all markers are checked during experimental validation and time synchronisation. Missing markers introduce errors in the computation of joint kinematics. Hence, several repetitions of trials may be necessary to ensure that the marker trajectory of each marker on the exoskeleton and joint kinematics of humans are entirely captured for comparison.

The kinematics of human joints, obtained from the Xsens Awinda system, and the kinematics of the exoskeleton structure, obtained from the marker trajectories of the BTS motion capture system, were analysed simultaneously. The data were linearly interpolated (normalised) to a common sampling frequency to match the sampling rates of Xsens data (60 Hz) and the BTS motion capture rate (250 Hz). The joint angles for each leg’s hip, knee, and ankle for humans and exoskeletons were plotted for multiple gait cycles. The variation between the human joint angles and exoskeleton joints during flexion/extension of the left and right legs is plotted in Figure 9. The patterns show that the exoskeleton joints fairly mimic the human joint angles during the complete gait duration.

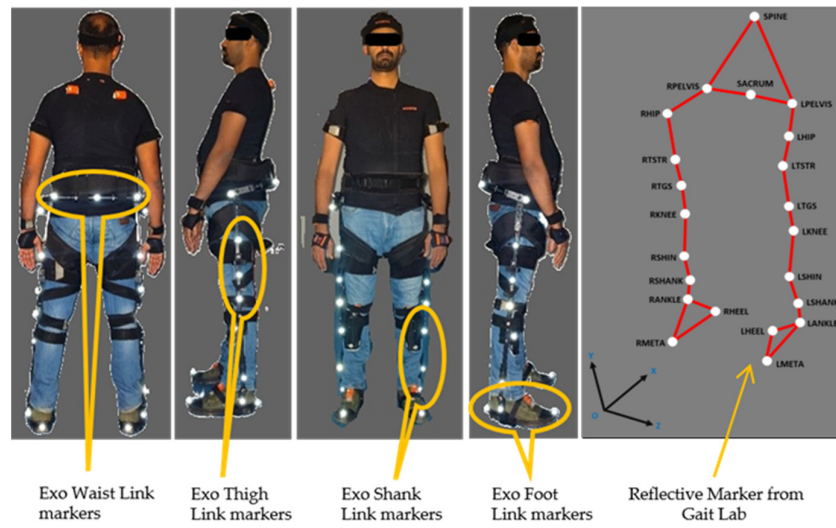


**Figure 8.** Experimental setup for simultaneous kinematic data collection of the human exoskeleton, with Xsens sensors on the human and reflective markers on the exoskeleton.

The comparison between the RMSD of simulation and experimental results for the flexion/extension of the hip, knee, and ankle joints for the left and right legs is presented in Table 3. The values reasonably match for the hip, knee, and ankle joints. The most significant deviation observed between the simulation and experiment is for the left knee joint. It could be attributed to some slippage of the straps on the thigh and shank that may have occurred for the left leg of the exoskeleton.

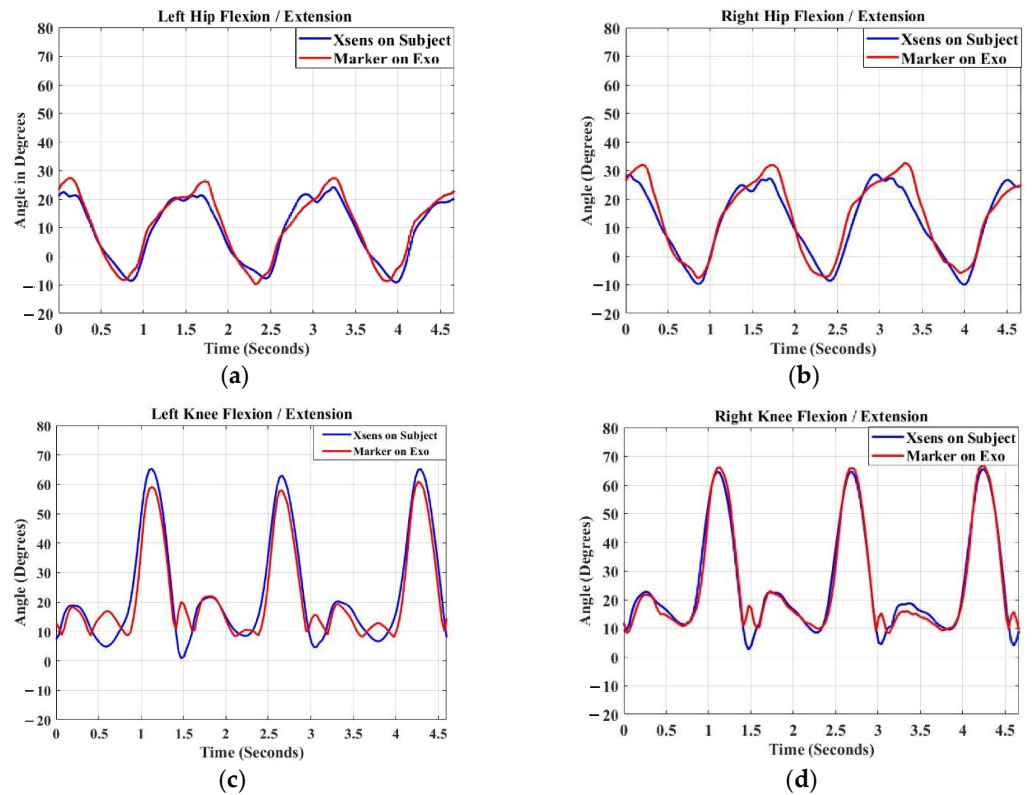


**Figure 9.** Cont.

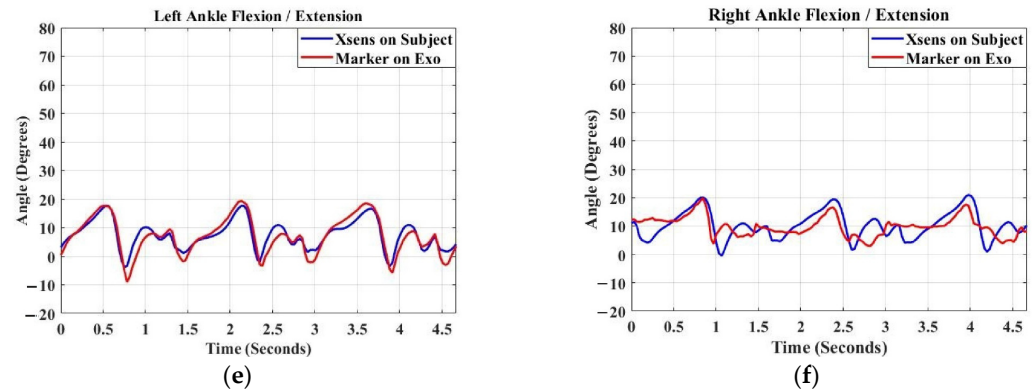


**Figure 9.** (a,b) The flexion–extension of the hip joint; (c,d) the flexion–extension of the knee joint; (e,f) the flexion–extension of the ankle joint. The blue curve is of the subject wearing the Xsens system, and the red curve is of the exoskeleton with passive markers in the BTS gait lab during experimental validation for multiple gait cycles.

**Table 3.** Comparison of RMSD of the human exoskeleton in simulation and experiment.

| Joint Angle Estimation Errors in Degree between Simulation and Experimental Approach |           |            |            |            |            |            |            |
|--|-----------|------------|------------|------------|------------|------------|------------|
|  |           | HIP F/E    |            | Knee F/E   |            | Ankle F/E  |            |
|  |           | Simulation | Experiment | Simulation | Experiment | Simulation | Experiment |
| RMSD   | Left Leg  | 5.5°       | 3.09°      | 0.5°       | 6.43°      | 1.4°       | 2.99°      |
|  | Right Leg | 6.4°       | 4.18°      | 0.6°       | 3.46°      | 1.4°       | 4.20°      |

#### 4. Discussion

An augmentative exoskeleton should increase the human’s strength or endurance without affecting the wearer’s natural movements. Incompatibility between the DOF of the anatomical joints and the joints of an exoskeleton can lead to unwanted forces and torques on the wearer, resulting in discomfort. However, the movements required for a particular task may employ only specific anatomical DOF, and hence, if an exoskeleton includes all possible DOF, it may be unnecessarily complex. The primary aim of this work was to develop a simulation-based framework for obtaining optimal compatibility of the human–exoskeleton system for specific tasks, in this case, walking on uneven terrain. The virtual modelling framework of the human–exoskeleton coupled system provides insights into the effect of various exoskeleton configurations on the wearer. It speeds up the development process for physical realisation by enabling rapid testing of multiple designs.

Configurations incorporating various DOFs at the hip, knee, and ankle—the primary joints involved in walking—were considered for the simulation. Subject-specific kinematic data for walking were used to drive a kinematic anthropomorphic model fitted with different configurations of the exoskeleton, and the RMSD between the joint movements of the human model and the exoskeleton was determined. While previous studies have understood the relationship between interaction forces and measures of misalignment [31], here, the focus is on the kinematics alone because the design of the exoskeleton is non-actuated, and the target population for its use is healthy, young soldiers walking on uneven terrain. The simulations were used to choose the DOF necessary for the exoskeleton design for performing the specific activity.

The simulations showed that the MaxDev (Table 2) for the chosen Config16 was 7.5° for ankle inversion/eversion on one side. The lack of abduction/adduction and internal/external rotation in the AnyBody human model was a limitation for the knee joint. Therefore, the exoskeleton configurations did not consider additional DOF at the knee joint. Despite this limitation, the maximum value of RMSD of the knee angles was 4.1° in

Config5, and it was  $0.5^\circ$  in the chosen Config16, indicating that for the specific activity of walking, the other DOF at the knee does not have a significant influence.

Further to the inferences derived from RMSD and deviation from Table 2, a similar inference has been derived considering the complete RoM of the human, RoM of the exoskeleton, and their deviations for the complete gait cycle for all configurations.

Further, the RoM of the human and exoskeleton joints for all 16 configurations have been plotted and presented in Figure S1 of Supplementary Materials, along with input reference joint motion trajectory. It is observed that the human joint trajectories were altered when coupled with different exoskeleton configurations. It is observed that extension of the human hip joint does not occur for configurations 6, 10, and 11 (Figure S1i,j). For config 5, 7, 8, and 11 with two DoF (FE, AbAd) at the hip joint of the exoskeleton, it is observed that the RoM of the exoskeleton hip joint is highly restricted irrespective of the RoM at the ankle joint (Figure S1w,x). The RoM of the human hip joint is between  $30^\circ$  and  $10^\circ$  in flexion and extension, respectively, for the other configurations. There is a sharp change in different joint angles in configuration 9, which may be due to the effect of the exoskeleton system on the human. Although the joint angles during left hip AbAd are between  $2^\circ$  and  $-6^\circ$ , the dispersion of the angles is highest between the midstance and pre-swing phases of gait (Figure S1g,h). It was observed that the internal rotation of the hip is more important than the abduction/adduction at the hip, which reduces the overall misalignment error.

From the profiles of the knee joint angles of the human, as shown in Figure 10a,b, it was observed that for certain configurations, the knee joints of the human tend to move into hyperextension. Hence, such configurations are eliminated, and the choice of configurations narrows down to Configuration 13, 14, and 16. Further, in conjunction with the reference from Table 2, config 13 is eliminated as it has the least CWS index, and hence the most suitable configurations are 14 and 16. The optimal configuration for the intended activity with the exoskeleton is configuration 16, followed by configuration 14.

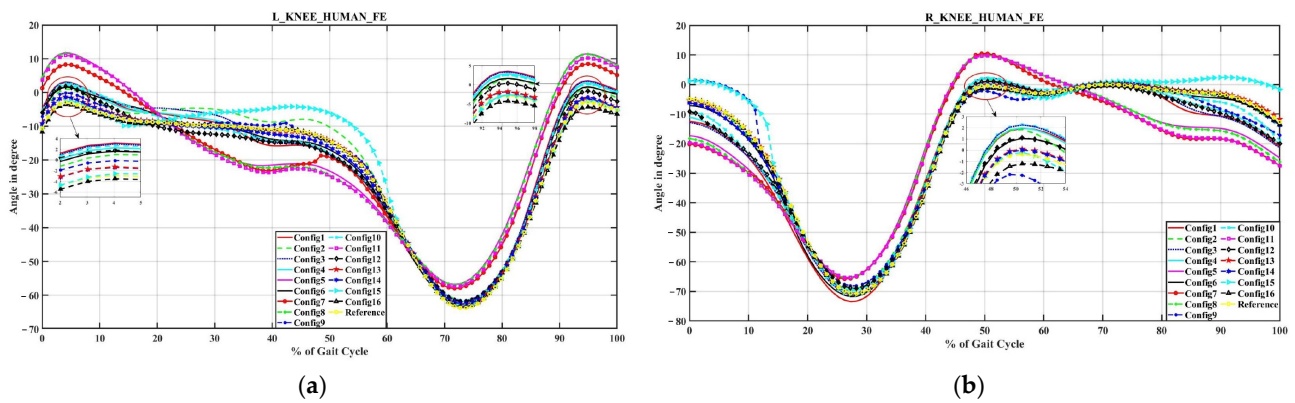


Figure 10. (a,b) The RoM of joint angles (knee) for human.

The deviation plots for all the configurations, as shown in Figure S2 of the Supplementary Materials, indicate that the deviation was maximum for configuration 7, which matches the inference from Table 2. The minimum deviations for configurations 1, 4, 14, and 16, as tabulated in Table 2, match the deviation profiles in Figure S2.

Configuration 16, with three DoF at the hip joint, one DoF at the knee joint, and three DoF at the ankle joint, was the optimal kinematically compatible configuration for walking on even and uneven surfaces. Although this configuration closely matches the DoF of the human joints, the simulation framework provides a quantitative approach to obtain the optimal configuration. Configuration 14 is also a good choice if the walking is restricted to even surfaces.

Further, to verify the robustness of the simulation, a detailed prototype was realised with this configuration and experimentally validated. Based on the initial exoskeleton design choices, the framework provides a generic approach to any chosen biomechanical

activity, mechanisms (traditional joints, self-aligning joints), and structure (rigid or flexible) envisaged. It would substantially reduce the development time and cost. It can also provide subject-specific insights and can enhance the scale of production. This methodology also quantitatively indicates the configurations that should be avoided.

The deviation profiles of the human–exoskeleton joint kinematics are indicated in Figure S3 of Supplementary Materials, which suggests that the deviations are repetitive for multiple gait cycles. The magnitude of the deviations depends on several factors, such as the fitment onto the subject, the tightness of coupling at the interfaces, and deviation in marker positions on the exoskeleton during the experiment.

An earlier experimental study for capturing the human and exoskeleton kinematics was performed by Torricelli et al. [13]. However, since they used the same motion capture system to capture the human and exoskeleton motions, they had to perform separate trials for each motion since the marker placements would be hidden otherwise. We could simultaneously capture the kinematics using two different systems in our work. The purpose of Torricelli et al. was to use the motion of the exoskeleton to drive the human joints for rehabilitation purposes. Our application is to ensure that the exoskeleton follows the wearer's motion.

The best kinematic configuration of the exoskeleton for walking on even and uneven terrain is Config 16, which has sufficient mobility at the hip and the ankle joint. Based on the RSMD criterion, the other optimal configurations are Config 1, Config 12, and Config 14. Based on the maximum deviation criterion, the other optimal configurations are Config 1, Config 4, and Config 14. Further, these configurations could be used ideally for specialised military and industrial applications where repeated tasks and load carriage are predominant. Config 14, with high mobility at the hip and restricted at the ankle joint, could be helpful for load augmentation on even terrains or terrains with uniform up slopes or down slopes. Config 12 has high mobility at the ankle joint and lesser mobility at the hip joint. It can find its application in industry for logistics and tasks that involve bending, lifting, or turning with load. In the military scenario, this configuration could carry a payload such as military equipment/personal protective gear, including bulletproof jackets and helmets. Config 4, with its restricted movement in the hip, can be used in scenarios where the hip movement needs to be restricted but with enough angle mobility. This configuration could be used in rescue operations during earthquakes, floods, and other natural disasters. Firefighters could also use it to carry heavy equipment during operations. Config 1 has high restrictions on the movement in the hip and ankle joints. It applies in scenarios where restricting movement is essential but requires load carriage. For instance, it can help carry heavy tools in a factory assembly line setup for an extended period. Other applications of these optimal configurations can be explored in industries that emphasise providing logistics support, warehouses, airports, dockyards, and railway stations where continuous material handling is necessary.

This simulation-based approach could be extended to different activities and a larger population. Musculoskeletal modelling and simulations are subject-specific, and the simulation framework and experimental validations on multiple subjects require computationally intensive resources and time. Hence, the simulation was performed for a particular activity on a single subject in this work, which is a limitation of this study and could be taken up in the future. Further, the experimental validation has been performed only on the chosen configuration. Experimental validations for all configurations require the development of an exoskeleton test bed, with the capability of locking/unlocking various joints to realise 16 different kinematic configurations, which would be part of future work. Another limitation is the choice of DoF considered at the knee joint when coupled with the AMS human model. The number of plausible configurations when the knee joint has three DoF is 64 configurations. However, this exercise will not be beneficial since the musculoskeletal model of AMS [26] has three DoF at the hip joint, one DoF at the knee joint, and two DoF at the ankle joint. Hence, even if other combinations with additional DOF at the knee joint were considered, they cannot be compared with the angles of the human model. The simulation-based

framework and the experimental validation were performed for walking on a level ground. However, the exoskeleton was developed to transfer the backpack load to the ground while walking on even and uneven terrain. Hence, while obtaining the best configuration of the exoskeleton, the system capable of walking on uneven ground is considered. As the input data for simulation and its subsequent experimental validation could not be performed on uneven terrain conditions, this could be considered a study limitation. As a part of the future scope, simultaneous kinematic data capture in field/outdoor conditions should be explored. Kinematic simulation of the human–exoskeleton-constrained system has only been performed without estimating interactive forces between human and exoskeleton systems. Simulation of interactive forces is computationally intensive, and experimental validation necessitates highly customised sensors and instrumentation for measurements.

## 5. Conclusions

Augmentative exoskeletons should provide unobstructed mobility to the wearer while augmenting the intended biomechanical activity. As it is challenging to mimic the exact mechanism of the human joints, the exoskeletons usually incorporate pseudo-anthropomorphic joints. Hence, the challenge is to finalise the best match of the exoskeleton from the various available options.

Hence, kinematic compatibility between human and exoskeleton systems is essential to achieve the intended outcome in augmentative applications. Generally, all exoskeletons are subject-specific, scenario-specific, and application-specific. Hence, when coupled with a musculoskeletal human model, a quantitative, simulation-based approach is essential to study the effects of various plausible kinematic configurations of the exoskeletons. Quantitatively simulating the best configuration provides an edge in the product development lifecycle, significantly reducing the time and effort taken to build, test, and iteratively improve the developmental prototypes. This approach provides the capability for mass production of an exoskeleton. A streamlined virtual coupled model would offer the complete kinematic data of the exoskeleton necessary for fitment and customisation.

The passive augmentative exoskeleton realised in this work was designed to enhance endurance and provide augmentation during walking on even and uneven surfaces. Hence, from the above analysis, the optimal configuration of the exoskeleton 16 has three DoF at the hip, one DoF at the knee, and three DoF at the ankle. The exact configuration is realised and experimentally tested for validation.

Further work can include other joint mechanisms (such as polycentric ones for the knees) for the different anatomical joints of the human body and for various activities. Compatibility of complaint mechanisms and redundancy studies for multiple configurations can be studied. A subject-specific framework can be quickly adapted to study the inter-subject variability for misalignment compensation strategies. Different activities of daily life that are specific to other scenarios, such as sitting to standing, squatting, kneeling, turning side to side, and stepping, can be analysed.

**Supplementary Materials:** The following supporting information can be downloaded at: <https://www.mdpi.com/article/10.3390/robotics13050079/s1>, Figure S1: (c–f) and (g–l) present the RoM of joint angles (ankle and hip) for human, and figures (m–z) present the RoM of joint angles (Hip, Knee, and Ankle) for exoskeleton. Figure S2: (a–l) present the deviation of joint angles (hip, knee, and ankle) for all configurations. Figure S3: Deviation between human and exoskeleton flexion/extension at hip, knee, and ankle joints from experimental validation.

**Author Contributions:** Conceptualisation, S.N., K.M. and S.S.; methodology, S.N. and S.S.; software, S.N.; validation, S.N. and K.M.; formal analysis, S.N. and S.S.; investigation, S.N. and K.M.; resources, K.M.; data curation, S.N. and K.M.; writing—original draft preparation, S.N.; writing—review and editing, S.S. and K.M.; visualisation, S.N. and K.M.; supervision, S.S. and K.M.; project administration, K.M.; funding acquisition, K.M. All authors have read and agreed to the published version of the manuscript.

**Funding:** This research received no external funding and the APC was funded by the authors.

**Institutional Review Board Statement:** The study was conducted in accordance with the Declaration of Helsinki and approved by the Institutional Ethics Committee of the Indian Institute of Technology Madras (IITM-IEC Protocol No.: IHEC/2020-02/SS/02/08).

**Data Availability Statement:** The data that support the findings of this study are available from the corresponding author upon reasonable request.

**Acknowledgments:** The material is based upon work supported by the Defence Research and Development Organisation (DRDO) under the Exoskeleton development program. The views and conclusions contained in this document are those of the authors and should not be interpreted as representing the official policies, either expressly or implied, of DRDO or the Indian Government. The authors thank U K Singh, Director General (Life Sciences), for his vision and guidance, and T M Kotresh, Director DEBEL, for his constant support and encouragement.

**Conflicts of Interest:** The authors declare no conflict of interest.

## References

- Zhou, J.-Y.; Liu, Y.; Mo, X.-M.; Han, C.-E.; Meng, X.-J.; Li, Q.; Wang, Y.-J.; Zhang, A. A preliminary study of the military applications and future of individual exoskeletons. *J. Phys. Conf. Ser.* **2020**, *1507*, 102044. [[CrossRef](#)]
- Shi, D.; Zhang, W.; Zhang, W.; Ding, X. A Review on Lower Limb Rehabilitation Exoskeleton Robots. *Chin. J. Mech. Eng.* **2019**, *32*, 74. [[CrossRef](#)]
- Golabchi, A.; Chao, A.; Tavakoli, M. A Systematic Review of Industrial Exoskeletons for Injury Prevention: Efficacy Evaluation Metrics, Target Tasks, and Supported Body Postures. *Sensors* **2022**, *22*, 2714. [[CrossRef](#)] [[PubMed](#)]
- Schmitt, D. Insights into the evolution of human bipedalism from experimental studies of humans and other primates. *J. Exp. Biol.* **2003**, *206*, 1437–1448. [[CrossRef](#)] [[PubMed](#)]
- Gull, M.A.; Bai, S.; Bak, T. A Review on Design of Upper Limb Exoskeletons. *Robotics* **2020**, *9*, 16. [[CrossRef](#)]
- Torricelli, D.; Del Ama, A.J.; Gonzalez, J.; Moreno, J.; Gil, A.; Pons, J.L. Benchmarking lower limb wearable robots: Emerging approaches and technologies. In Proceedings of the 8th ACM International Conference on Pervasive Technologies Related to Assistive Environments, Cofru, Greece, 1–3 July 2015; pp. 2–5. [[CrossRef](#)]
- Lajeunesse, V.; Vincent, C.; Routhier, F.; Careau, E.; Michaud, F. Exoskeletons' design and usefulness evidence according to a systematic review of lower limb exoskeletons used for functional mobility by people with spinal cord injury. *Disabil. Rehabil. Assist. Technol.* **2015**, *11*, 535–547. [[CrossRef](#)] [[PubMed](#)]
- Zhang, B.; Liu, T.; Pecht, M.G. Recent Development of Unpowered Exoskeletons for Lower Extremity: A Survey. *IEEE Access* **2021**, *9*, 138042–138056. [[CrossRef](#)]
- Yu, S.; Han, C.; Cho, I. Design considerations of a lower limb exoskeleton system to assist walking and load-carrying of infantry soldiers. *Appl. Bion. Biomech.* **2014**, *11*, 119–134. [[CrossRef](#)]
- Dollar, A.M.; Herr, H. Lower Extremity Exoskeletons and Active Orthoses: Challenges and State-of-the-Art. *IEEE Trans. Robot.* **2008**, *24*, 144–158. [[CrossRef](#)]
- Young, A.J.; Ferris, D.P. State of the Art and Future Directions for Lower Limb Robotic Exoskeletons. *IEEE Trans. Neural Syst. Rehabil. Eng.* **2017**, *25*, 171–182. [[CrossRef](#)] [[PubMed](#)]
- Mallat, R.; Khalil, M.; Venture, G.; Bonnet, V.; Mohammed, S. Human-exoskeleton joint misalignment: A systematic review. In Proceedings of the 2019 Fifth International Conference on Advances in Biomedical Engineering (ICABME), Tripoli, Lebanon, 17–19 October 2019; pp. 1–4.
- Torricelli, D.; Cortés, C.; Lete, N.; Bertelsen, Á.; Gonzalez-Vargas, J.E.; Del-Ama, A.J.; Dimbwadyo, I.; Moreno, J.C.; Florez, J.; Pons, J.L. A Subject-Specific Kinematic Model to Predict Human Motion in Exoskeleton-Assisted Gait. *Front. Neurobot.* **2018**, *12*, 18. [[CrossRef](#)] [[PubMed](#)]
- Cenciarini, M.; Dollar, A.M. Biomechanical considerations in the design of lower limb exoskeletons. In Proceedings of the 2011 IEEE International Conference on Rehabilitation Robotics, Zurich, Switzerland, 29 June–1 July 2011; pp. 1–6.
- Herr, H. Exoskeletons and orthoses: Classification, design challenges and future directions. *J. Neuroeng. Rehabil.* **2009**, *6*, 21. [[CrossRef](#)] [[PubMed](#)]
- Yandell, M.B.; Quinlivan, B.T.; Popov, D.; Walsh, C.; Zelik, K.E. Physical interface dynamics alter how robotic exosuits augment human movement: Implications for optimizing wearable assistive devices. *J. Neuroeng. Rehabil.* **2017**, *14*, 40. [[CrossRef](#)] [[PubMed](#)]
- Näf, M.B.; Junius, K.; Rossini, M.; Rodriguez-Guerrero, C.; Vanderborght, B.; Lefeber, D. Misalignment Compensation for Full Human-Exoskeleton Kinematic Compatibility: State of the Art and Evaluation. *Appl. Mech. Rev.* **2018**, *70*, 050802. [[CrossRef](#)]
- Gálvez-Zúñiga, M.A.; Aceves-López, A. A Review on Compliant Joint Mechanisms for Lower Limb Exoskeletons. *J. Robot.* **2016**, *2016*, 5751391. [[CrossRef](#)]
- Stienen, A.H.A.; Hekman, E.E.G.; van der Helm, F.C.T.; van der Kooij, H. Self-Aligning Exoskeleton Axes Through Decoupling of Joint Rotations and Translations. *IEEE Trans. Robot.* **2009**, *25*, 628–633. [[CrossRef](#)]
- Cempini, M.; De Rossi, S.M.M.; Lenzi, T.; Vitiello, N.; Carrozza, M.C. Self-Alignment Mechanisms for Assistive Wearable Robots: A Kinetostatic Compatibility Method. *IEEE Trans. Robot.* **2012**, *29*, 236–250. [[CrossRef](#)]

21. Jarrasse, N.; Morel, G. Connecting a Human Limb to an Exoskeleton. *IEEE Trans. Robot.* **2011**, *28*, 697–709. [[CrossRef](#)]
22. Bartenbach, V.; Wyss, D.; Seuret, D.; Riener, R. A lower limb exoskeleton research platform to investigate human-robot interaction. In Proceedings of the 2015 IEEE International Conference on Rehabilitation Robotics (ICORR), Singapore, 11–14 August 2015; pp. 600–605.
23. Zanotto, D.; Akiyama, Y.; Stegall, P.; Agrawal, S.K. Knee Joint Misalignment in Exoskeletons for the Lower Extremities: Effects on User's Gait. *IEEE Trans. Robot.* **2015**, *31*, 978–987. [[CrossRef](#)]
24. Schepers, M.; Giuberti, M.; Bellusci, G. Xsens MVN: Consistent Tracking of Human Motion Using Inertial Sensing. *Xsens. Technol.* **2018**, *1*, 1–8. [[CrossRef](#)]
25. Karatsidis, A.; Jung, M.; Schepers, H.M.; Bellusci, G.; de Zee, M.; Veltink, P.H.; Andersen, M.S. Musculoskeletal model-based inverse dynamic analysis under ambulatory conditions using inertial motion capture. *Med. Eng. Phys.* **2019**, *65*, 68–77. [[CrossRef](#)] [[PubMed](#)]
26. Carbone, V.; Fluit, R.; Pellikaan, P.; van der Krogt, M.M.; Janssen, D.; Damsgaard, M.; Vigneron, L.; Feilkas, T.; Koopman, H.F.J.M.; Verdonchot, N. TLEM 2.0—A comprehensive musculoskeletal geometry dataset for subject-specific modeling of lower extremity. *J. Biomech.* **2015**, *48*, 734–741. [[CrossRef](#)] [[PubMed](#)]
27. Damsgaard, M.; Rasmussen, J.; Christensen, S.T.; Surma, E.; de Zee, M. Analysis of musculoskeletal systems in the AnyBody Modeling System. *Simul. Model. Pract. Theory* **2006**, *14*, 1100–1111. [[CrossRef](#)]
28. Roetenberg, D.; Luinge, H.; Slycke, P. Xsens MVN: Full 6DOF human motion tracking using miniature inertial sensors. *Xsens Motion Technol. BV Tech. Rep.* **2009**, *1*, 1–7.
29. Breloff, S.P.; Wade, C.; Waddell, D.E. Lower extremity kinematics of cross-slope roof walking. *Appl. Ergon.* **2018**, *75*, 134–142. [[CrossRef](#)] [[PubMed](#)]
30. Wannop, J.W.; Worobets, J.T.; Ruiz, R.; Stefanyshyn, D.J. Footwear traction and three-dimensional kinematics of level, downhill, uphill and cross-slope walking. *Gait Posture* **2014**, *40*, 118–122. [[CrossRef](#)] [[PubMed](#)]
31. Bessler-Etten, J.; Schaake, L.; Prange-Lasonder, G.B.; Buurke, J.H. Assessing effects of exoskeleton misalignment on knee joint load during swing using an instrumented leg simulator. *J. Neuroeng. Rehabil.* **2022**, *19*, 13. [[CrossRef](#)] [[PubMed](#)]

**Disclaimer/Publisher's Note:** The statements, opinions and data contained in all publications are solely those of the individual author(s) and contributor(s) and not of MDPI and/or the editor(s). MDPI and/or the editor(s) disclaim responsibility for any injury to people or property resulting from any ideas, methods, instructions or products referred to in the content.